Non-symmetric approach to single-screw expander and compressor modeling

IOP Conf. Series: Materials Science and Engineering **232** (2017) 012076 doi:10.1088/1757-899X/232/1/012076

Non-symmetric approach to single-screw expander and compressor modeling

Davide Ziviani[1,2], Eckhard A. Groll[2], James E. Braun[2], W. Travis Horton[2], M. De Paepe[1], M. van den Broek[1]

[1]Department of Flow, Heat, and Combustion Mechanics, Ghent University - UGent Sint-Pietersnieuwstraat 41, 9000 Gent, Belgium
[2]Purdue University, School of Mechanical Engineering, Ray W. Herrick Laboratories, West Lafayette, IN, USA

E-mail: davide.ziviani@ugent.be, groll@purdue.edu, jbraun@purdue.edu, wthorton@purdue.edu, martijn.vandenbroek@ugent.be, michel.depaepe@ugent.be

Abstract. Single-screw type volumetric machines are employed both as compressors in refrigeration systems and, more recently, as expanders in organic Rankine cycle (ORC) applications. The single-screw machine is characterized by having a central grooved rotor and two mating toothed starwheels that isolate the working chambers. One of the main features of such machine is related to the simultaneous occurrence of the compression or expansion processes on both sides of the main rotor which results in a more balanced loading on the main shaft bearings with respect to twin-screw machines. However, the meshing between starwheels and main rotor is a critical aspect as it heavily affects the volumetric performance of the machine. To allow flow interactions between the two sides of the rotor, a non-symmetric modelling approach has been established to obtain a more comprehensive model of the single-screw machine. The resulting mechanistic model includes in-chamber governing equations, leakage flow models, heat transfer mechanisms, viscous and mechanical losses. Forces and moments balances are used to estimate the loads on the main shaft bearings as well as on the starwheel bearings. An 11 kWe single-screw expander (SSE) adapted from an air compressor operating with R245fa as working fluid is used to validate the model. A total of 60 steady-steady points at four different rotational speeds have been collected to characterize the performance of the machine. The maximum electrical power output and overall isentropic efficiency measured were 7.31 kW and 51.91%, respectively.

1. Introduction

Single-screw machines are widely employed as compressors and more recently as expanders in organic Rankine cycle applications [1, 2].

One of the main features of such machines is that the meshing between the main rotor and the starwheels (or gaterotors) generates identical working chambers on both sides of the main rotor with benefits on the loads acting on the main shaft bearings, as shown in Figure 1. The common approach to model the single-screw machine is to consider only one side of the compressor or expander with multiple control volumes according to the number of grooves [3]. The authors proposed a comprehensive mechanistic model of a single-screw expander accounting for the wrapping of the grooves at the end of expansion process [4].

Nomenclature

c_v	Specific Heat at Constant Volume (J kg^{-1} K^{-1})
D	Diameter (m)
h	Specific Enthalpy (kJ/kg)
	Heat Transfer Coefficient (kW/m^2K)
i	Transmission Ratio (-)
m	Mass (kg)
$\dot{m}$	Mass Flow Rate (kg/s)
p	Pressure (kPa)
$\dot{Q}$	Heat Rate (kW)
T	Temperature (K)
u	Specific Internal Energy (kJ/kg)
v	Specific Volume (m^3/kg)
V	Volume (m^3)
$\dot{W}$	Power (W)
$\mathbf{v}$	Velocity Vector (m/s)
w	Tooth width (m)
z	Number of Grooves or Teeth (-)
η	Efficiency (-)
ρ	Density (kg/m^3)
θ	Rotation Angle (rad)
ω	Angular Speed (rad/s)

Subscript

amb	ambient
CV	Control Volume
ex	discharge
exp	expander
el	electric
eff	effective
fr	friction
g	groove
loss	losses
mech	mechanical
nom	nominal
su	suction
sh	shaft

In the case of an expander, the discharge process is important to evaluate under or over expansion losses.

The majority of the research works have considered the expansion process until discharge opening without including the complete evolution of each groove. The authors extended the original mechanistic model to include the full evolution of each groove during one working cycle in [5, 6]. Preliminary CFD results of a single-screw expander under transient conditions showed that the pressure distributions at the suction inlet are not identical due to the internal ducting pressure drops as well as because the two sides of the rotor are not fully isolated [7]. For these reasons, a non-symmetric approach to model single-screw machines is proposed within this work with the aim of estimating the indicated power (p-V work rate), the friction losses and the mechanical efficiency. A SSE with an 11 kWe generator, shown in Figure 2, with a 122 mm rotor is used as reference case. The expander performance was characterized my using R245fa as working fluid.

2. Mechanistic Model

The single-screw expander is divided into ten control volumes (CVs) of which six are associated with working chambers (i.e., grooves) and their volumes change according to the rotation angle. The remaining static control volumes are associated with the common inlet, the two ducts leading to the suction ports and the discharge shell volume. The different control volumes are visible in Figure 1. A polygon approach is applied to both starwheels to obtain the tooth areas mating with the corresponding grooves, as shown Figure 3. The polygon approach is also used to obtain all the geometric information of the expander such as volume curves, porting areas, leakage path lengths and groove surfaces. Such procedure is outlined in details in [5, 8]. The complete volume curve evolution as well as the areas of suction and discharge ports are reported in Figure 4.

To handle the complexity of the geometry model and the multi-control volumes, a multi-layer solution scheme has been developed. The conceptual schematic of the algorithm is shown in Figure 5. Once the simulation is initialized with the boundary conditions and input data, the geometric properties calculated are stored. For each control volume cycle integration is carried out by using an adaptive solver that adjusts the step taken according to the stiffness of the

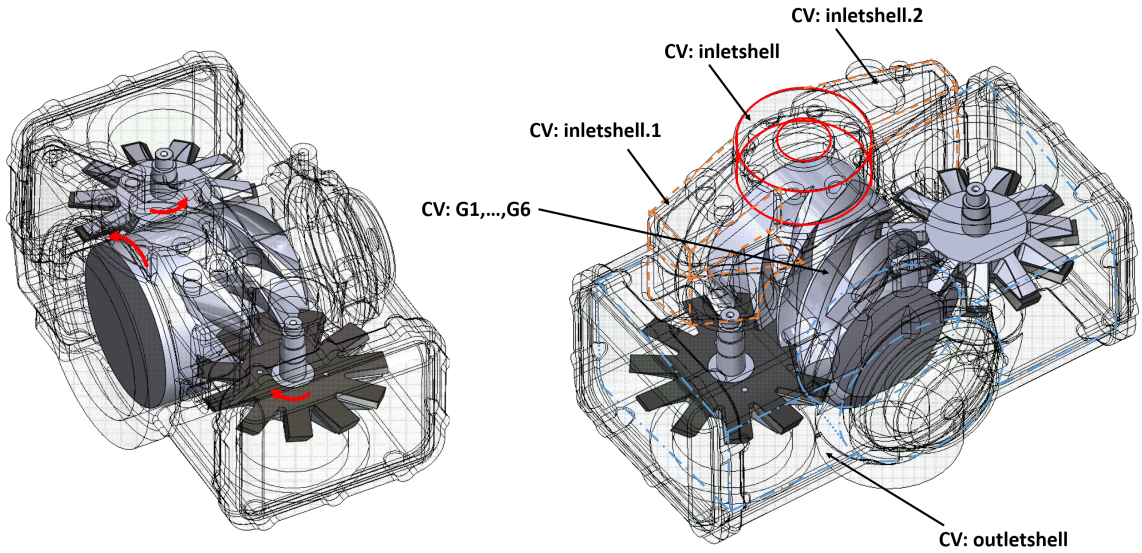

Figure 1. Transparent 3D view of the single-screw machine: with rotating directions (left) and identifications of the control volumes.

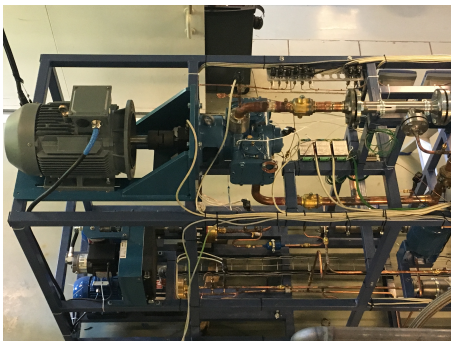

Figure 2. 11 kWe single-screw expander considered in the present study.

Table 1. Main geometric parameters of 11 kWe single-screw expander.

Engaging ratio	[-]	11/6
D_{sr}	[mm]	122
D_{sw}	[mm]	132
$V_{g,max}$	[cm^3]	57.39
$r_{v,built-in}$	[-]	5.3
L_{rotor}	[m]	121

problem. The cycle includes suction and discharge flow models, inlet tube models accounting for pressure drops and heat transfer with the housing walls, in-chamber heat transfer and the state variable derivatives. Once the cycle has converged, forces, moments, boundary work rate and friction losses are computed and an overall energy balance is enforced.

2.1. Governing Equations

The conservation equations of mass and energy are applied simoultaneously to each control volume to obtain the change in thermodynamic states. The properties within a control volume are assumed to be uniform, i.e. gradients within compressor chambers are neglected. Temperature and density have been chosen as independent thermodynamic properties to take advantage of the equation of state implementation in the CoolProp library [9]. For each control volume, the general conservation of mass equation can be written as:

$$\frac{d(\rho V)_{CV}}{d\theta} = \frac{1}{\omega}\sum_i \dot{m}_i \tag{1}$$

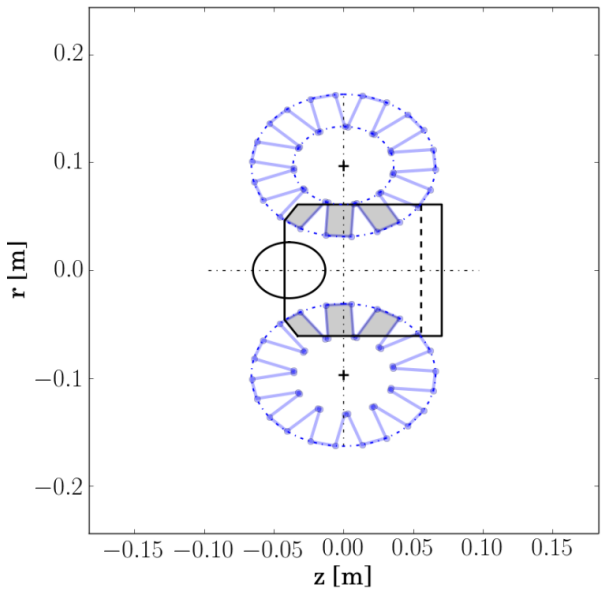

Figure 3. Planar representation of single-screw geometry with polygon approach (adapted from [6]).

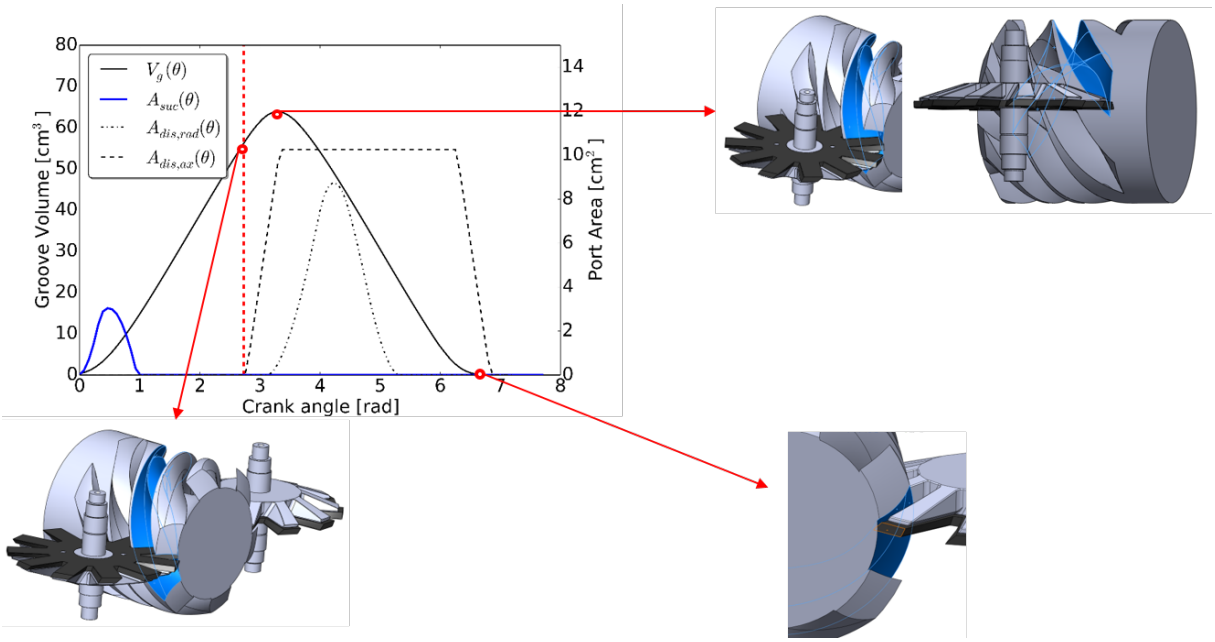

Figure 4. Groove volume and port area evolution with respect to the main rotor crank angle. 3D CAD views help visualize discharge opening, maximum groove volume and discharge end situations.

The general conservation of energy in each chamber of the compressor can be rearranged to obtain the derivative of temperature with respect to the crank angle [10]:

$$m_{CV} c_v \frac{dT}{d\theta} = -T \left(\frac{\partial p}{\partial T} \right)_v \left[\frac{dV}{d\theta} - v \frac{dm_{CV}}{d\theta} \right] - h \frac{dm_{CV}}{d\theta} + \frac{\dot{Q}}{\omega} + \frac{1}{\omega} \sum_i (\dot{m}h)_i \qquad (2)$$

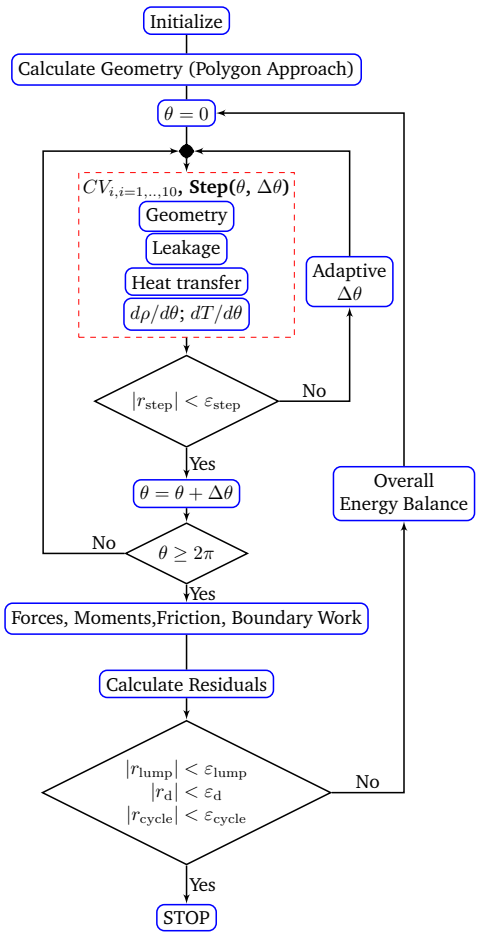

Figure 5. Solution algorithm of the single-screw mechanistic model.

where the mass in the control volume is given by $m_{CV} = (\rho V)_{CV}$.

In a single-screw machine, there are nine main leakage paths as described by Ziviani et al. [4]. The leakage paths can be divided into three types:

- constant clearance gap: leading and trailing edges of the grooves, gap between starwheel disk and housing and end of groove band;
- variable clearance gap: sealing lines of the teeth.
- orifice type: blow holes between tooth and groove due to wear of the profile or non-perfect milling process.

An isentropic flow through nozzle with proper flow coefficient is used to model gaps associated with wear, as they are quite difficult to accurately predict. For the remaining leakage paths, the flow model is still used, but a detailed 1D compressible flow model [11] has been employed to estimate the correction factor, M, between isentropic flow and flow with friction:

$$M = \frac{\dot{m}_{\text{nozzle}}}{\dot{m}_{\text{1D,fr}}} = \frac{a_0 \left(L/L_0\right)^{a_1}}{a_2 \left(\delta/\delta_0\right) + a_3} \left[\xi \left(a_4 Re^{a_5} + a_6\right) + \left(1 - \xi\right) \left(a_7 Re^{a_8} + a_{10}\right)\right] + a_{10} \tag{3}$$

where the dimensionless characteristic length and dimensionless gap width are given by $L^* = L/L_0$ and $\delta^* = \delta/\delta_0$ with L_0 and δ_0 being the reference length and gap width values.

The average boundary work rate generated by the expander is calculated as

$$\overline{\dot{W}}_{pV} = \frac{\omega}{2\pi}\int_0^{2\pi} p(\theta)\frac{\mathrm{dV}}{d\theta}d\theta \tag{4}$$

The average mechanical power output of the expander is obtained by subtracting the mechanical losses from the boundary work rate:

$$\dot{W}_{\mathrm{mech}} = \overline{\dot{W}}_{pV} - \dot{W}_{\mathrm{mech,loss}} \tag{5}$$

where the mechanical losses are obtained by solving the forces and moments balance equations for starwheel and main rotor [6], shown in Figure 6. The mechanical torque of the main shaft is determined by decomposing the gas force distribution along the groove on the Y-Z and X-Z planes [12].

Thus, the mechanical efficiency of the expander is calculated as the ratio of the mechanical shaft power to the boundary work rate (or indicated power):

$$\eta_{\mathrm{mech}} = \frac{\dot{W}_{\mathrm{mech}}}{\overline{\dot{W}}_{pV}} \tag{6}$$

The overall energy balance of the expander housing is written as,

$$\dot{W}_{\mathrm{mech,loss}} + \sum_i \dot{Q}_i(T_{\mathrm{lump}}) = 0 \tag{7}$$

where T_{lump} is the mean temperature of the lumped mass of the expander shell and $\dot{Q}_i$ represents all the heat transfer interaction terms between the different parts of the expander and the shell. In the present model, a single-lumped temperature is used and Equation (6) reduces to:

$$\dot{W}_{\mathrm{mech,loss}} + \overline{\dot{Q}}_{CV,wall} + \dot{Q}_{inletshell,wall} + \dot{Q}_{outletshell,wall} + UA_{\mathrm{amb}}\left(T_{\mathrm{amb}} - T\right) = 0 \tag{8}$$

where the average value of the overall heat transfer coefficient UA_{amb} has been determined by calibrating a semi-empirical model of the expander on the experimental data [13].

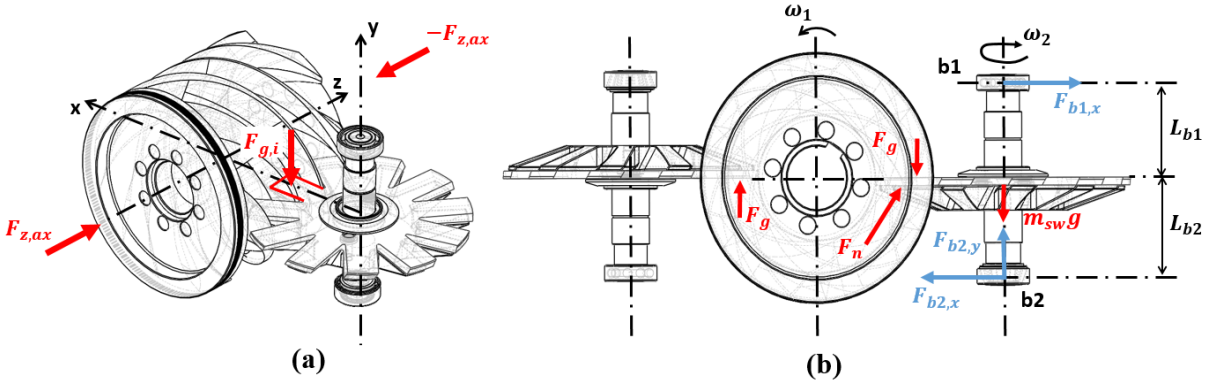

Figure 6. Schematic of the forces on main rotor and starwheels (adapted from [6]).

Table 2. Minimum and maximum values of the measured and derived variables for the single-screw expander with rotational speeds of 2000 rpm and 3000 rpm running with R245fa.

	$p_{su,exp}$ (kPa)	$T_{su,exp}$ (°C)	$p_{ex,exp}$ (kPa)	$T_{ex,exp}$ (°C)	$\dot{m}_r$ (kg/s)	r_p (-)	r_v (-)	$\dot{W}_{exp,el}$ (W)	$\varepsilon_{is,oa,exp}$ (-)	φ_{FF} (-)
Min	566	106.7	120	75.5	0.12	3.71	3.76	1283	0.2058	0.938
Max	1230	124.9	232	104.6	0.37	7.26	7.74	7364	0.5191	1.231

3. Experimental Data

The experimental characterization of the considered single-screw expander has been discussed in [13]. For the sake of compactness, the minimum and maximum values of the measured and calculated variables for two rotational speeds are reported in Table 2. The expander was directly connected to a generator and inverter. The electrical power output as a function of the expansion specific volume ratio is shown in Figure 7. The maximum electric power output measured is 7.364 kW at an overall isentropic efficiency of 51.91%. To be noted is that there are two groups of data at 3000 rpm due to variations of the condensing temperatures.

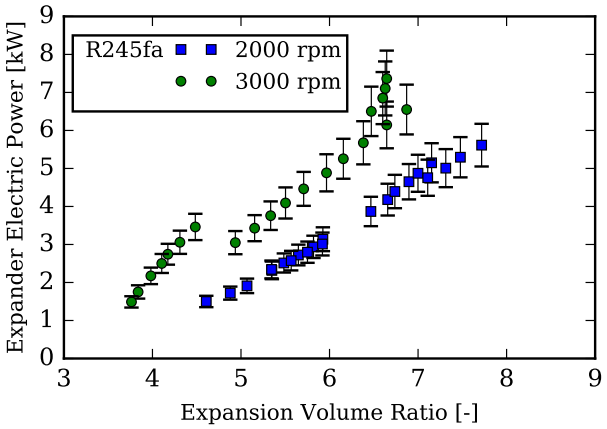

Figure 7. Expander electric power out as function of the expansion volume ratio for R245fa at different rotational speeds. The steady-state points at 2000 rpm and 3000 rpm are displayed. Uncertainty bars of the power output are overlaid.

4. Results and Discussion

The usefulness of the mechanistic model is related to its capability of estimating the mechanical losses associated with both friction as well as leakage flows.

As only the electrical power out has been measured, the combined electro-mechanical and heat losses can be estimated. An overall energy balance on the expander and electric equipment is performed and the sum of heat losses and electro-mechanical losses, $\dot{W}_{el-m,loss}$, can be calculated as:

$$\dot{Q}_{amb,exp,loss} + \dot{W}_{el-m,loss} = \dot{m}_r \left(h_{su,exp} - h_{ex,exp}\right) - \dot{W}_{el,grid,exp} \tag{9}$$

where the enthalpy difference across the expander is obtained by the measured temperature and pressure values upstream and downstream the expander. The resulting losses are shown in Figure 8(a).To be noted is that the energy balance is closed with significant losses compared to the power output. Moreover, the total losses decreases with the increase of the pressure ratio.

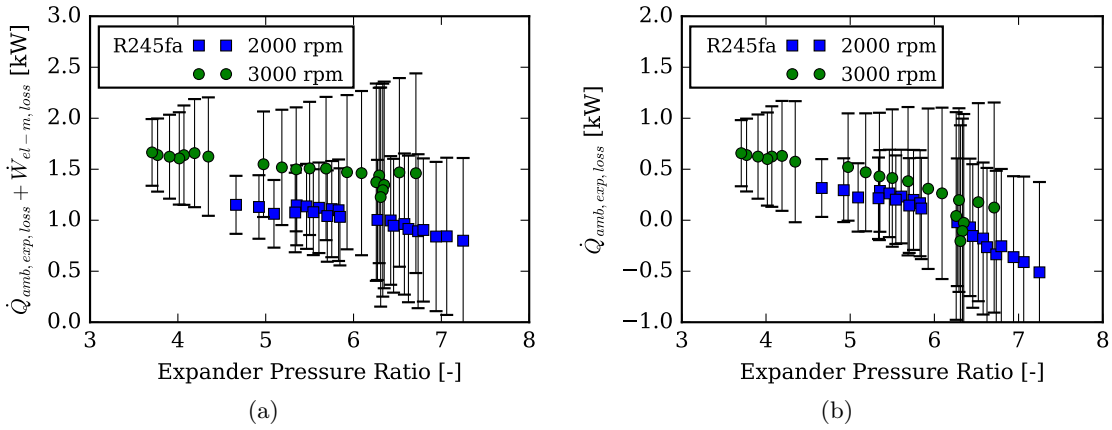

Figure 8. (*a*) Overall energy balance of the expander; (*b*) estimation of the expander heat losses through the housing.

In fact, as the power output increases, the efficiency of the electric equipment increases as well. In addition, the contribution of the decrease in electrical-mechanical losses is more significant compared to the heat losses through the housing since the inlet temperature of the working fluid was kept close to 125 °C for the majority of the experimental points.

As different source of losses are included in such energy balance, the performance map of generator and inverter have been determined in order to isolate the heat losses through the expander housing. This is accomplished by performing an energy balance only on the expander:

$$\dot{Q}_{amb,exp,loss} = \dot{m}_r \left(h_{su,exp} - h_{ex,exp}\right) - \dot{W}_{mech} \tag{10}$$

The heat rate loss values and the associated uncertainties are reported in Figure 8(b). For some of the experimental points, the heat losses are slightly negative. This fact is certainly associated with the accuracy of the performance map used to back up the expander shaft power.

The mechanistic model is employed here to estimate the mechanical shaft power and to obtain the actual mechanical efficiency by including the friction power losses associate with the bearings and friction contacts between teeth and grooves. Therefore the mechanistic model is first validated with a set of experimental data. The resulting parity plots between calculated and experimental points are shown in Figure 9.

The validated model has been exercised to calculate the boundary work rate and the friction losses for each of experimental conditions. The results are reported in Figure 10(a). In particular, the filled markers represents the boundary work rate for two rotational speeds. By applying Equation 4, suction pressure losses are accounted for. The indicated efficiency contributions can be estimated by including the leakage losses. The total friction losses are overlaid in the same figure with empty markers. To be noted is that the friction losses represent a significant contribution to decrease the expander power output. In fact, the mechanical efficiency is estimated to be around 70% for expander pressure ratios between 5 and 7, near optimum operating conditions for the given internal volume ratio and internal pressure drops [2]. Such high friction losses have been associated with the non-sufficient lubrication between tooth and starwheel as well as the bearings. After a detailed inspection, the injection orifices were found partially occluded. Additionally, the tooth profiles were worn out, suggesting high wear.

To further validate the mechanistic model, dynamic pressure transducers have been installed in different points of the housing to capture the entire expansion process. The experimental work is currently ongoing on a new set of rotor and meshing pair of starwheels.

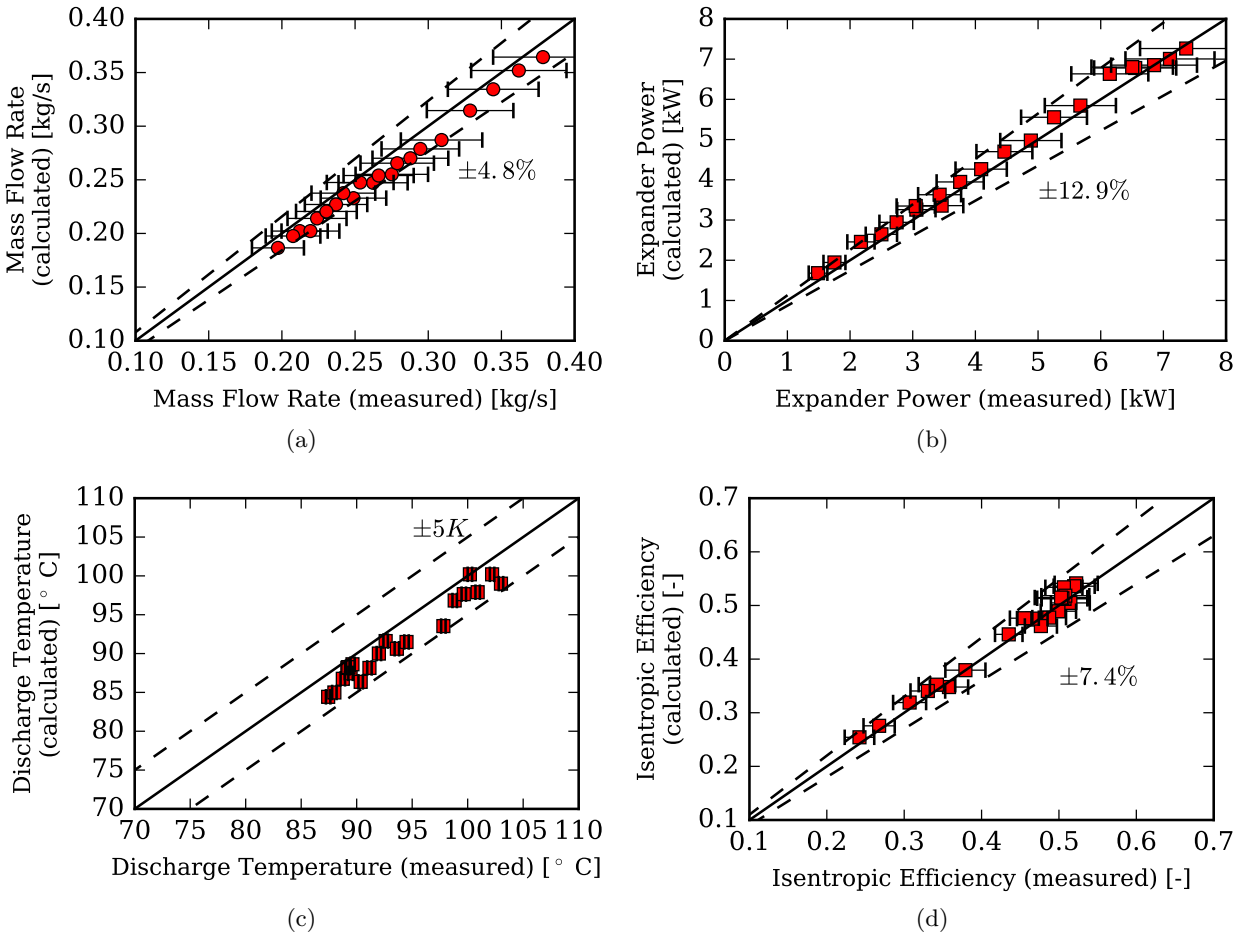

Figure 9. Non-symmetric single-screw expander model parity plots: (a) mass flow rate; (b) electric power output; (c) expander discharge temperature; (d) overall isentropic efficiency. A total of 21 steaty-state points are shown at 3000 rpm. Uncertainty bars are over laid. The maximum relative error is reported in each plot.

5. Conclusions

In this paper, a non-symmetric approach to modeling single-screw machines has been presented. Such approach accounts for the working process occurring on both sides of the rotor and possible interactions between the working chambers. A single-screw expander in an ORC application has been used to validate the model and to estimate the total friction losses and expander mechanical efficiency. the model predicted a maximum mechanical efficiency of approximately 70%. The trade-off between complexity of the model and accuracy will be evaluated by employing dynamic pressure sensors to record the indicated diagram of the expander.

Acknowledgments

The authors would like to acknowledge Sergei Gusev for the extensive experimental campaign carried out as well as thank the Center of High Performance Building (CHPB) for sponsoring the project entitled "Development of general purpose simulation tools for positive displacement compressors".

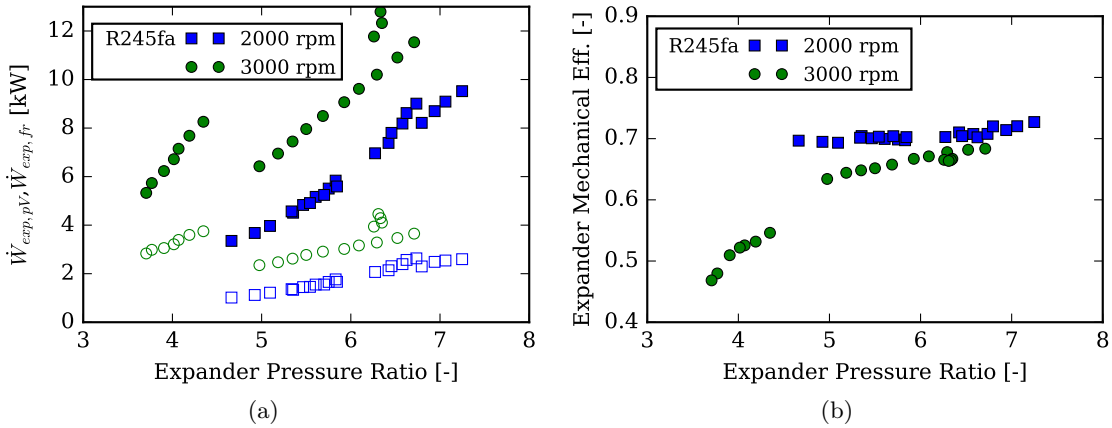

Figure 10. (*a*) Calculated boundary work rate (filled markers) and friction power losses (empty markers) as a function of the applied pressure ratio; (*b*) calculated mechanical efficiency of the expander.

References

[1] Wei Wang B L, Wu Y T, Ma C F, J-F W, Zhang L, Li C, Zhao Y K and Zhi R P 2016 *Energy* **116** 43–52

[2] Ziviani D, Sergei S, Lecompte S, Groll E A, Braun J E, Horton W T, van den Broek M and De Paepe M 2017 *Applied Energy* **189** 416–432

[3] Bein T W and Hamilton J F 1982 Computer modeling of an oil flooded single screw air compressor *International Compressor Engineering Conference* paper 383

[4] Ziviani D, Bell I H, De Paepe M and van den Broek M 2014 Comprehensive model of a single screw expander for orc-systems applications *22th Int.Compressor Engineering Conf. at Purdue* 1506

[5] Ziviani D, Bell I, M D P and van den Broek M 2015 Update on single-screw expander geometry model integrated into an open-source simulation tool *9th Int. Conf. on Compressors and their Systems, City University of London, London* 39

[6] Ziviani D, Bell I H, De Paepe M and van den Broek M 2016 Mechanistic model of an oil-flooded single-screw expander *23th Int.Compressor Engineering Conference at Purdue* 1486

[7] Ziviani D, Suman A G J, Pinelli M, De Paepe M and van den Broek M 2016 Cfd approaches applied to a single-screw expander *23th Int.Compressor Engineering Conference at Purdue* 1488

[8] Ignatiev K M 2012 Approach to the numeric geometry analysis of positive displacement compressors, its application to a single screw compressor simulation and verification by experiment *International Compressor Engineering Conference* 2059

[9] Bell I H, Wronski J, Quoilin S and Lemort V 2014 *Ind. Eng. Chem. Res.* **53** 2498–2508

[10] Bell I H 2011 *Theoretical and Experimental Analysis of Liquid Flooded Compression in Scroll Compressors* Ph.D. thesis Purdue Univeristy

[11] Bell I H, Groll E A, Braun J E and Horton W T 2013 *Int. J. Refrigeration* **36** 1965–1973

[12] Wu Y R and Tran V T 2016 *International Journal of Refrigeration* **65** 111–128

[13] Ziviani D, Sergei S, Lecompte S, Groll E A, Braun J E, Horton W T, van den Broek M and De Paepe M 2016 *Applied Energy* **181** 155–170